

Using mathematical modelling to identify data requirements for increased prediction accuracy in radiotherapy

Thomas D. Lewin^{1,*}, Philip K. Maini¹, Eduardo G. Moros², Jimmy Caudell², Heiko Enderling^{2,3,*}, and Helen M. Byrne^{1,*}

¹Wolfson Centre for Mathematical Biology, Mathematical Institute, University of Oxford, UK

²Department of Radiation Oncology, H. Lee Moffitt Cancer Center & Research Institute, USA

³Department of Integrated Mathematical Oncology, H. Lee Moffitt Cancer Center & Research Institute, USA

*tomlewin@hotmail.co.uk or heiko.enderling@moffitt.org or helen.byrne@maths.ox.ac.uk

ABSTRACT

Longitudinal gross tumour volume (GTV) clinical data from head and neck cancer patients show that tumours of a similar size and stage pre-treatment may respond very differently to the same radiotherapy fractionation protocol. Mathematical models of radiation response are often proposed as a means to predict treatment outcome and prescribe more personalised fractionation protocols. Predictive mathematical models aimed towards clinical applications should be sufficiently detailed to capture the range of dynamics observed *in vivo* while being sufficiently simple such that the model parameters are identifiable with respect to the data typically available for model calibration.

In this paper we show that models describing the spatiotemporal heterogeneity of the intratumoural composition may better capture observed *in vivo* dynamics than those describing the evolution of the tumour volume alone. We compare the range of qualitative responses with respect to GTV data throughout radiotherapy treatment to those observed in a cohort of head and neck cancer patients. Synthetic data studies are used to address questions of identifiability and uncertainty quantification. Our results argue that, to develop accurate, predictive mathematical models, there is a simultaneous need for more detailed models (possibly incorporating some notion of tumour heterogeneity) along with more sophisticated data metrics with which to inform such models.

Introduction

Radiotherapy remains a mainstay of cancer treatment, with approximately half of all cancer patients worldwide receiving radiotherapy as part of their treatment¹. Typically, treatment protocols are determined by tumour etiology, location and stage. Other patient-specific factors that may be important in determining therapeutic outcome, such as intrinsic radiosensitivity, hypoxic or necrotic areas, are not currently used to inform protocol selection in the clinic². Clinical data suggest that patients with similar tumour, node and metastasis (TNM) stage, and comparable tumour volumes prior to treatment may respond differently to the same radiotherapy fractionation schedule^{3,4}. Mathematical models may provide insights into cancer dynamics and also predict patient-specific responses to a given radiotherapy protocol. It is hoped that such models could eventually be used to prescribe improved fractionation schedules for each patient *a priori* or adaptively during the 5-7 weeks course of radiation⁵.

Any predictive mathematical model for use in the clinic should be suitable for purpose. It should incorporate sufficient biological detail to capture the observed responses *in vivo*, whilst balancing model complexity such that patient-specific model parameters may be calibrated from the data typically available in the clinic⁶⁻⁸. These issues are central to this paper and the models developed herein.

Computed tomography (CT) scans are routinely used in the clinic to image tumours at the diagnosis and treatment planning stages⁹⁻¹¹. Further scans, such as cone beam CT (CBCT), may be taken upon the delivery of each fraction but are most commonly used solely for alignment purposes. Additionally, the imaging modalities used are not necessarily of high resolution and do not differentiate the heterogeneity in composition between different intra-tumoural regions. As such, *in vivo* clinical data with which to calibrate mathematical models is typically limited and gross tumour volume (GTV) measurements may contain sources of error that are difficult to quantify.

As a result of this limited data availability, mathematical models aimed towards clinical applications are often relatively simple; involving few model parameters that need to be estimated^{12,13}. Consequently, such models may incorporate limited biological detail, often just considering the evolution of the GTV^{4,12}.

A common approach for existing mathematical models developed for this purpose is to describe the tumour volume dynamics using phenomenological differential equations^{12,14-19}. That is, the functional forms for the growth and/or radiotherapy response dynamics are motivated by empirical observations rather than resulting from more mechanistic derivations. They thus may not take into account potentially complex interactions and heterogeneity within the tumour microenvironment which may vary between patients and dynamically over time and may significantly influence the treatment outcome. A number of authors have proposed more complex, mechanistic models for tumour growth and radiotherapy response which demonstrate the impact that different forms of intratumoural heterogeneity may have on the resultant dynamics²⁰⁻²³. The challenge in this field is thus to balance the need for sufficient biological detail while minimising model complexity.

In this paper, we propose that mathematical models which solely describe the evolution of a homogeneous tumour volume may not be sufficient to capture the observed range of responses across the entire patient population. We show that a model incorporating some notion of intratumoural heterogeneity may better describe the full range of dynamics. We use synthetic data studies to further address the issues of parameter identifiability and uncertainty quantification of model predictions. We present data from a clinical dataset of head and neck cancer patients, highlighting cases by which to benchmark the range of dynamics captured by mathematical models, and suggest an extension of an existing model to a new two compartment ordinary differential equation (ODE) model describing the evolution of a dynamic, heterogeneous tumour. We show how the two compartment model may better capture the full range of dynamics observed *in vivo* and investigate the identifiability of the two compartment model with respect to the clinical data available. Finally, we use synthetic data from a more complex, mechanistic model of tumour growth and radiotherapy response to consider questions of experimental design with regards to improving parameter identifiability and the accuracy of model predictions.

Methods

In this section we provide an overview of the data, models, and parameter estimation techniques used throughout this paper. For further details, please see the supplementary material and the associated references.

Tumour volume data

As discussed previously, predictive mathematical models should be compatible with the data available for model calibration and assessing the quality of model predictions. That is, they should capture the range of observed dynamics while also being minimally complex such that the model may be reliably parametrised. Current best practice in the clinic involves two CT (computed tomography) scans for each patient - one at diagnosis and one at the treatment planning stage. These scans can then be used to estimate gross tumour volume⁹⁻¹¹. It is feasible to obtain further scans at the time of delivery of each fraction, but these scans are often of low quality and used only to position the patient and not stored for research purposes.

In this paper we use retrospective volumetric data collected weekly from head and neck cancer patients with a mixture of sites including the oropharynx, tonsil and base of tongue. Each CT scan was segmented by the same person, giving weekly tumour volumes throughout treatment, a volume measurement at the treatment planning stage for all patients and an additional measurement at diagnosis. The patient data shown in Figures 1 and 2 are those first presented in Lewin *et al.*²¹. The data shown in Figure 3 are from a cohort of nine head and neck cancer patients treated at the Moffitt Cancer Center, Florida. All methods were carried out in accordance with the institutional policies of the Moffitt Cancer Center and the University of Oxford. The clinical protocol covering patient data and methods used in this paper was approved by the Moffitt Cancer Center's Institutional Review Board (IRB). Since this is a retrospective study using de-identified data of adult human subjects, informed consent was waived by the IRB.

Broadly speaking, we observe several different classes of qualitative response within the clinical data. From a modelling point of view, these are response dynamics which we may hope to reproduce accurately from our model and even predict from pre-treatment/initial data. We highlight and characterise some of these response types in Figure 1.

In Figure 1a the patient responds well to radiotherapy with the tumour decreasing markedly in volume throughout the treatment. We refer to this type of behaviour hereafter as a 'fast responder'. By contrast, there are patients for whom the effects of radiotherapy appear to be marginal when viewed as tumour volume over time alone, as is the case in Figure 1b. We classify these patients as 'poor responders'. In a number of cases, the initial response of the tumour to radiotherapy appears to be favourable, but the response plateaus in the latter stages of treatment resulting in a non-negligible final tumour volume (Figure 1c). However, this radiographic volume may subsequently recede in the weeks after radiotherapy. Occasionally, as in Figure 1d, a patient may appear to exhibit continued tumour progression throughout the first few weeks of radiotherapy before showing a delayed response characterised by a decrease in tumour volume towards the end of treatment. We characterise this type of response as 'pseudo-progression'.

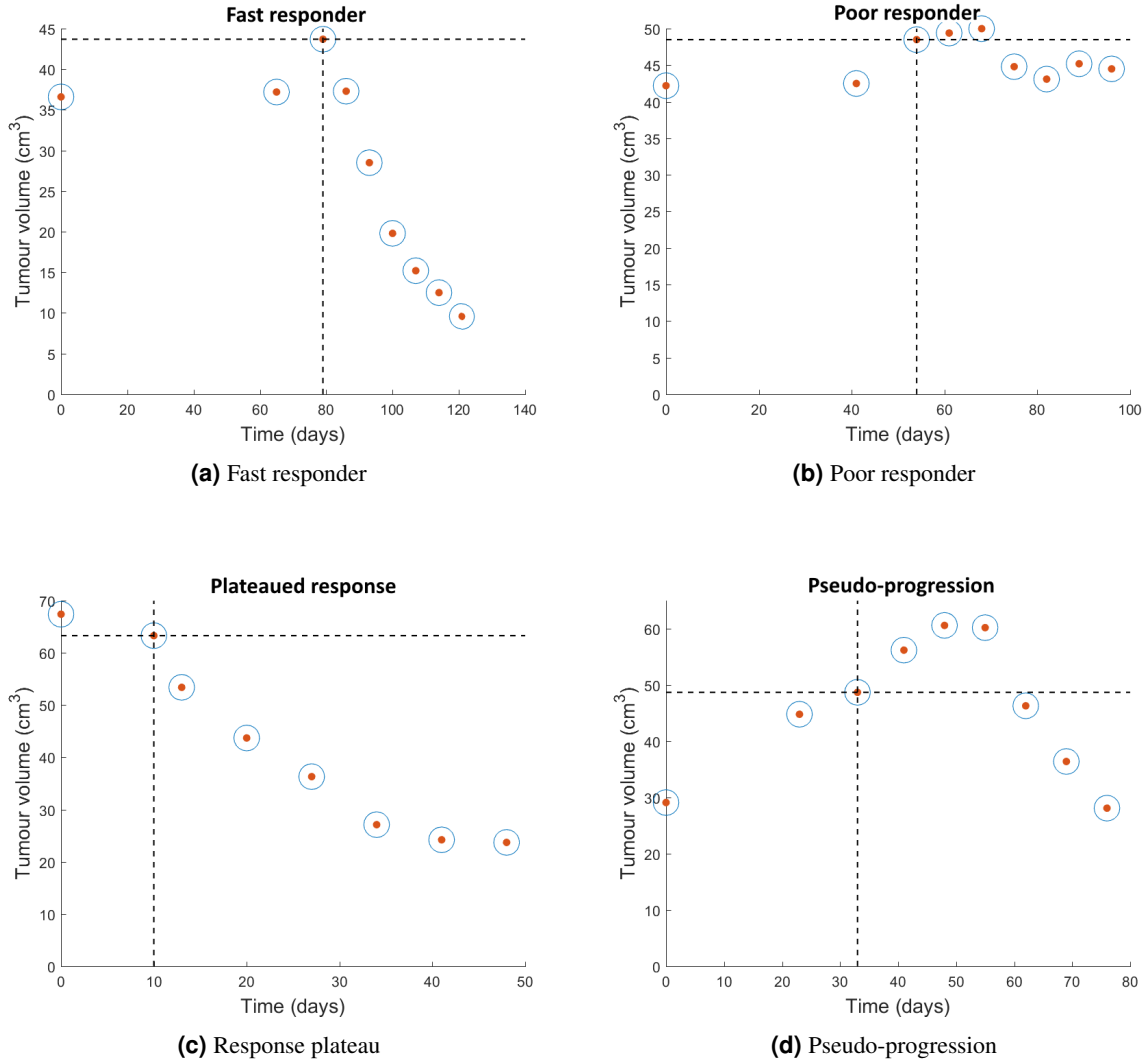


Figure 1. Representative examples of four qualitatively different radiotherapy response dynamics. The gross tumour volumes were obtained from pre-radiation treatment planning scans and weekly CBCT scans during treatment. Clinical data points are marked by the red filled circles. Dashed black lines indicate the start of treatment.

Tumour growth and treatment response models

Various methodologies have been employed in order to model tumour growth and radiotherapy response, including compartmental ODE models^{4, 12, 16–18, 24–26}, continuum partial differential equation (PDE) models^{19, 20, 22, 27}, computational agent-based models^{28–33} and probabilistic approaches^{34–39}. Simple, deterministic models are often proposed for clinical applications and are the focus of this paper. Phenomenological ODE models provide a high-level description of the tumour dynamics, aiming to describe the observed behaviour without accounting for much of the complex underlying biology. As such, these models tend to have relatively few parameters which may be more easily estimated from the potentially limited available data.

The simplest tumour growth models comprise a single ODE to describe the tumour volume dynamics. There are a number of phenomenological growth laws which have been proposed to provide a spatially averaged description for the change in tumour volume, including exponential, logistic, generalised logistic, and Gompertz growth terms^{14, 40–42}. Each of these models for tumour growth may be extended to account for radiotherapy, the simplest approach being to assume instantaneous cell death upon irradiation. Several authors have proposed models of this type and here we state one such model proposed by Prokopiou *et al.*¹² which forms the basis for comparison in this paper.

$$\frac{dV}{dt} = \lambda V \left(1 - \frac{V}{K}\right) - \sum_{i=1}^n \gamma V \left(1 - \frac{V}{K}\right) \delta(t - t_i) \quad (1)$$

The model of Prokopiou *et al.*, given by Equation (1), has been proposed for patient-specific prediction of tumour response to radiotherapy. Tumour growth is governed by the logistic growth law, while response to radiotherapy is incorporated as an instantaneous effect which also takes the logistic functional form with therapy applied at times t_i for $i = 1, \dots, n$. Experimental and clinical studies have demonstrated that tumour growth is most applicably modelled by growth laws with sigmoidal shapes, such as logistic growth or Gompertzian growth^{43,44}. The choice of logistic growth for this study is motivated by the shape of the clinical data⁴⁵. This model further assumes that the tumour growth rate, λ , and radiation-induced death rate, γ , are uniform population-level parameters. The carrying capacity, K , is assumed to be a patient-specific parameter which may be estimated from data, with the tumour volume to carrying capacity ratio at the start of treatment, referred to as the Proliferation Saturation Index, PSI, being proposed as a prognostic indicator of radiotherapy response^{4,12,15}. We note that, for ease of comparison, in this paper the data for each patient are treated separately and thus all estimated parameters are patient-specific.

However, models such as this may not capture the full range of dynamics observed *in vivo* (cf. Figure 1). Indeed it is straightforward to observe from Equation (1) that the instantaneous cell death term precludes the type of non-monotonic response observed in Figure 1d, for example. We propose that incorporating more biological detail with some notion of intratumoural heterogeneity may be required to better explain such dynamics and thus produce more accurate patient-specific predictions. Motivated by our previous work²¹, we hypothesise that heterogeneity in tumour composition may affect growth dynamics and, consequently, radiotherapy response. Furthermore, we anticipate that such heterogeneity is likely to be dynamic throughout the course of the radiotherapy protocol due to the widespread cell death induced upon irradiation. We thus consider a two compartment extension to the model in Equation (1), decomposing the tumour volume into a viable tumour cell population, V , and a volume comprised of non-viable cells and necrotic debris, N , such that the total tumour volume at time t is given by $V(t) + N(t)$. The subsequent model equations are given by

$$\frac{dV}{dt} = \lambda V \left(1 - \frac{V}{K}\right) - \eta V - \gamma \sum_{i=1}^n V \delta(t - t_i), \quad (2)$$

$$\frac{dN}{dt} = \eta V - \zeta N + \gamma \sum_{i=1}^n V \delta(t - t_i). \quad (3)$$

In this model viable tumour cells are assumed to undergo logistic growth with growth rate λ and carrying capacity K . Additionally, viable tumour cells become non-viable (or undergo necrosis) at a constant rate η . The non-viable material is assumed to undergo exponential decay at constant rate ζ . The effects of radiotherapy are included as an instantaneous transfer of mass between the viable tumour volume, V , and the non-viable compartment, N , for fractions delivered at times t_i . We assume that the dead material is unaffected by radiotherapy and so model radiation-induced cell death as proportional to the viable tumour cell compartment, V , with death rate γ , in contrast to Equation (1) whereby the logistic term is assumed to encompass the population of cells sensitive to irradiation.

Coupled with appropriate initial conditions for the viable and non-viable volumes, $V(0)$ and $N(0)$, Equations (2) and (3) define our two compartment model for tumour growth and radiotherapy response. We note that this model is similar in form to those proposed by other authors^{17,18,24}. This model is presented here as a simple extension to the scalar ODE model presented in Equation (1) in order to facilitate model comparison and the discussion of the issues that are the focus of this paper; the specific forms of the model equations are of lesser importance.

In order to better understand the influence of incorporating heterogeneity in the two compartment model and to facilitate consideration of questions regarding identifiability and experimental design we further use a more complex mechanistic model of tumour growth and radiotherapy response to provide a ‘ground truth’ for synthetic data. Synthetic data for both total tumour volume and intratumoural necrotic volume are generated using different parameter regimes from the multiphase model developed in our previous work^{21,46} to replicate the qualitative dynamics shown in Figure 1. In this context we interpret ‘ground truth’ data as being provided by a known, more detailed mathematical model for which all the aspects of the underlying tumour dynamics are known and quantifiable. Such data are used as hypothetical clinical data that include information on intratumoural heterogeneity. Further details of the multiphase model may be found in the supplementary material and the original references^{21,46}.

Model calibration

The central motivation of this paper concerns the issue of calibrating predictive mathematical models in the clinic. Numerous methodologies may be employed to estimate model parameters with respect to a given dataset⁴⁷⁻⁵⁰.

In contrast to most optimisation approaches, Bayesian techniques for parameter inference allow us to generate probability distributions rather than point estimates. For any given model, the highly heterogeneous nature of the tumour micro-environment that leads to variations in the measured variable of interest (including inter-patient variability), uncertainty and sources of noise inherent in the data, and even uncertainty in the model itself means that it is natural to consider each parameter as a

random variable rather than a fixed point estimate of some ‘true’ value. While computationally more expensive, the extra information gained about the underlying distributions of each parameter make Bayesian methods useful in assessing a model with respect to data. For example, we may more readily quantify the uncertainty of any model predictions or identifiability of model parameters.

These considerations motivate our choice of approach. In this paper we make use of a Bayesian technique known as the Approximate Bayesian Computation Sequential Monte Carlo (ABC SMC) algorithm^{51,52}. We mitigate some of the issues raised by Alahmadi *et al.*⁵³ with an appropriate termination threshold for the algorithm to take into account the noise in the clinical data. Further simulations using a complementary approach yielded unchanged results (not shown). For more technical details see the supplementary material and the references therein.

Results

Capturing clinical dynamics

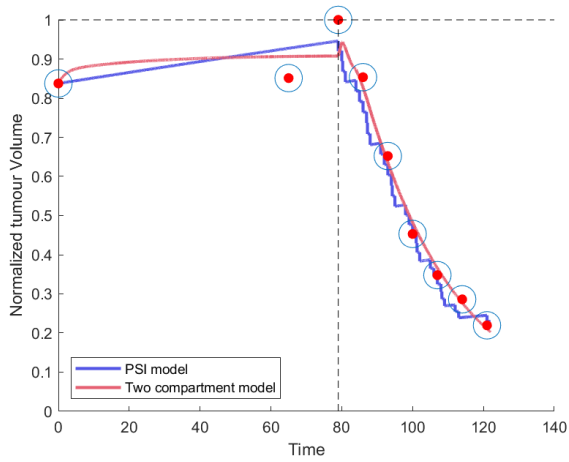
As described in the methods section, simple scalar ODE models may not capture the full range of radiotherapy responses observed *in vivo* as described by changes in GTV. The additional biological detail and heterogeneity described by the two compartment model, given by Equations (2) and (3), results in a wider range of dynamics, including tumour volume trajectories qualitatively similar to those displayed in Figure 1 (results shown in supplementary material). Indeed, fitting individual parameter sets for both the PSI model and the two compartment model to the examples in Figure 1 we observe that, while the PSI model may adequately describe the data for the ‘fast’ and ‘poor’ responder dynamics (Figures 2a and 2b), only the two compartment model is able to capture the more complex, non-linear responses referred to as the ‘response plateau’ and ‘pseudo-progression’ cases (Figures 2c and 2d). This is perhaps not surprising given the simplicity of Equation (1) and in light of our previous work which investigated the dependency of such dynamics on the spatiotemporal heterogeneity of tumour composition²¹.

We proceed to further investigate the performance of the two compartment model by considering the uncertainty in the model predictions after calibration to the individual patient data across our dataset. In Figure 3 we plot 95% credible intervals from the posterior predictive distribution for both total tumour volume, $V(t) + N(t)$, and the underlying necrotic volume, $N(t)$ for each patient. For each patient we may observe a reasonably good fit to the data with tight credible intervals for total tumour volume predictions. However the large credible intervals for the necrotic volume for these patients suggest that the model is unidentifiable with respect to the calibration data with large uncertainty in the underlying tumour composition dynamics. For example, for the patient represented in the top left panel of Figure 3 we see that the 95% credible interval suggests that the initial necrotic fraction of the tumour may be anywhere from 50% of the GTV to 0. Moreover, the response to treatment shown by the patient in the bottom left panel may equally be captured by a tumour composed almost entirely of necrotic tissue or almost entirely of viable tumour cells by the end of treatment. Indeed, examination of the pairwise marginal densities from the posterior distribution of parameters for such patients demonstrates this lack of identifiability and correlations between model parameters. In Figure 4 we visualise the pairwise posterior parameter distributions and marginal densities resulting from fitting the two compartment model to the first patient in our dataset (shown in the top left panel of Figure 3). The lime green data points represent the regions of highest density in the posterior distribution. Visualising the posterior distribution in this manner reveals correlations between estimated model parameters and large uncertainties in certain parameter values, in particular for the carrying capacity, K , and initial necrotic fraction, $\Phi_0 = N_0/(N_0 + V_0)$.

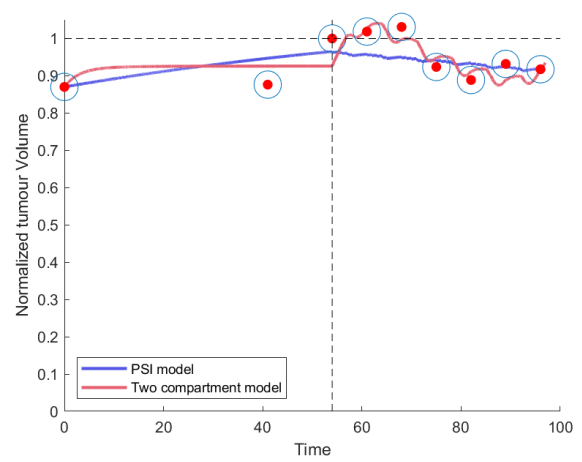
Identifiability and experimental design

While the greater range of dynamics exhibited by the two compartment model appears promising, the results of the previous section raise questions about parameter identifiability with respect to typically available clinical data. In this section we use synthetic data studies to address questions of experimental design for determination of an appropriate dataset to allow sufficient model calibration. Synthetic data are generated from a more detailed, mechanistic multiphase model of heterogeneous tumour growth and radiotherapy response developed in our previous work^{21,46} in the manner described in the supplementary material for use as a ‘ground truth’.

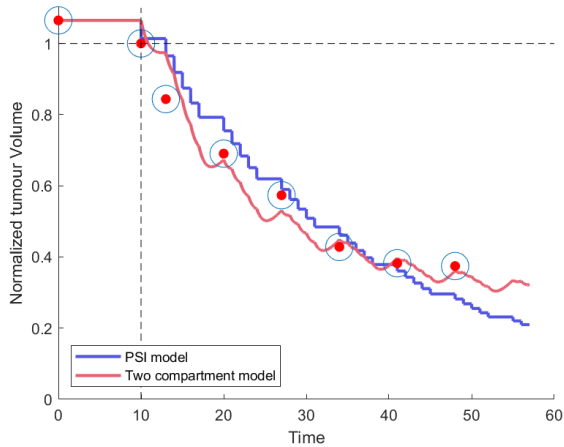
The results of the previous section suggest that simply increasing the temporal resolution of GTV measurements would not improve the practical identifiability of the two compartment model proposed. As such, we instead consider a hypothetical scenario in which the scans enabling GTV measurements for each patient in our dataset are also sufficient to measure the tumour volume fraction which is comprised of regions of necrosis or dead cellular material. We simulate this scenario using synthetic data generated from our multiphase model⁴⁶ to obtain datasets with the same temporal resolution as our clinical data but twice the total number of data points which incorporate information on the underlying heterogeneity. More specifically, we choose parameter regimes for the multiphase model which qualitatively reproduce the plateau and pseudo-progression dynamics.



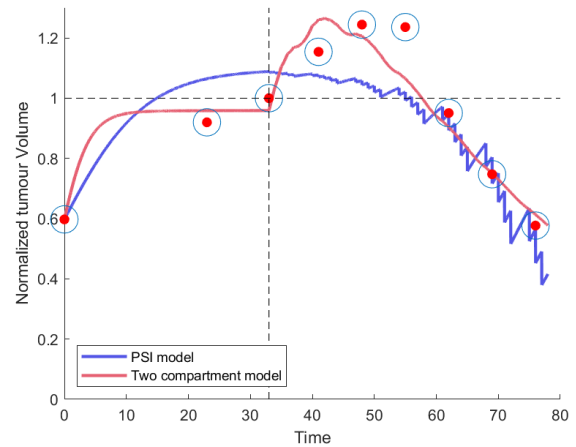
(a)



(b)



(c)



(d)

Figure 2. The best-fitting solutions for the PSI model given by Equation (1) (blue) and two compartment model given by Equations (2) and (3) (red) using the ABC SMC algorithm to fit to head and neck gross tumour volume clinical data throughout radiotherapy treatment. Clinical data points are marked by the red filled circles. Panels (a)-(d) correspond to cases (a)-(d) in Figure 1, respectively. Dashed black lines indicate start of treatment with each dataset normalised to the tumour volume at the start of treatment.

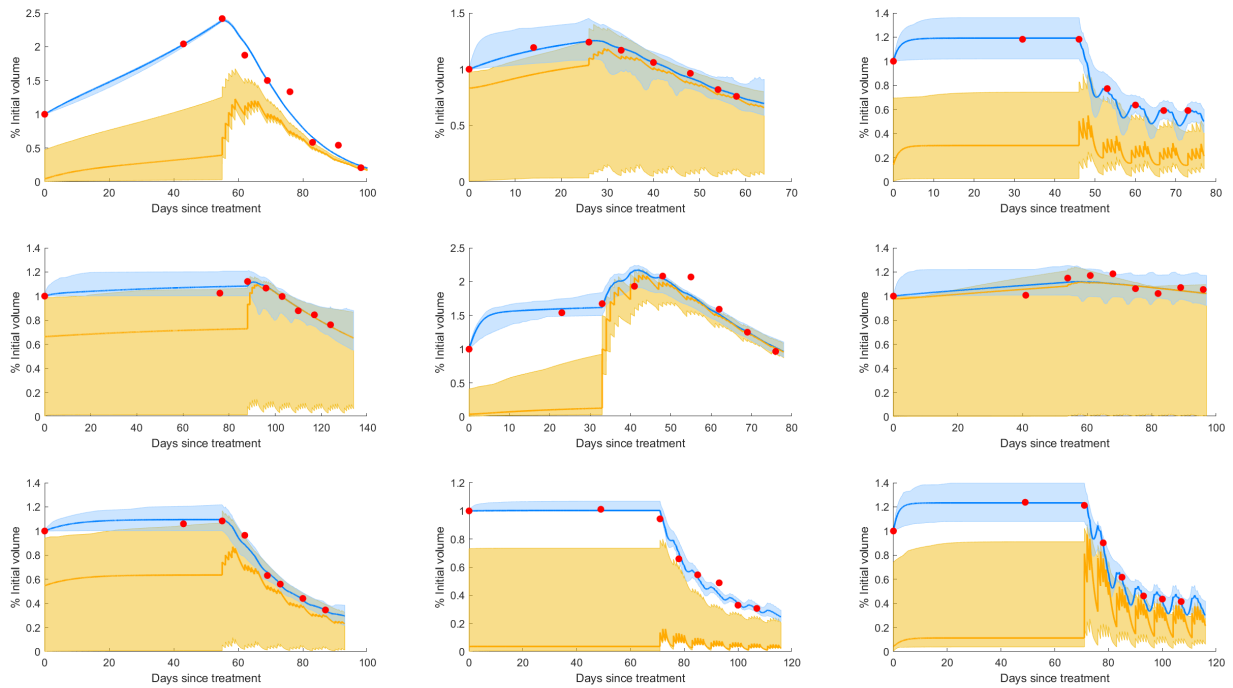


Figure 3. Results from fitting the two compartment model to 9 patients individually from our cohort of clinical patient data using the ABC SMC algorithm. The total tumour volume and underlying necrotic volume corresponding to simulations using the best-fitting parameter sets are shown by the blue and yellow curves, respectively. 95% credible intervals for the total tumour volume (blue regions) and underlying necrotic volume (yellow regions) at each time point are obtained by sampling 120 parameter combinations from the posterior distributions and simulating Equations (2) and (3). Clinical data points are marked by the red filled circles.

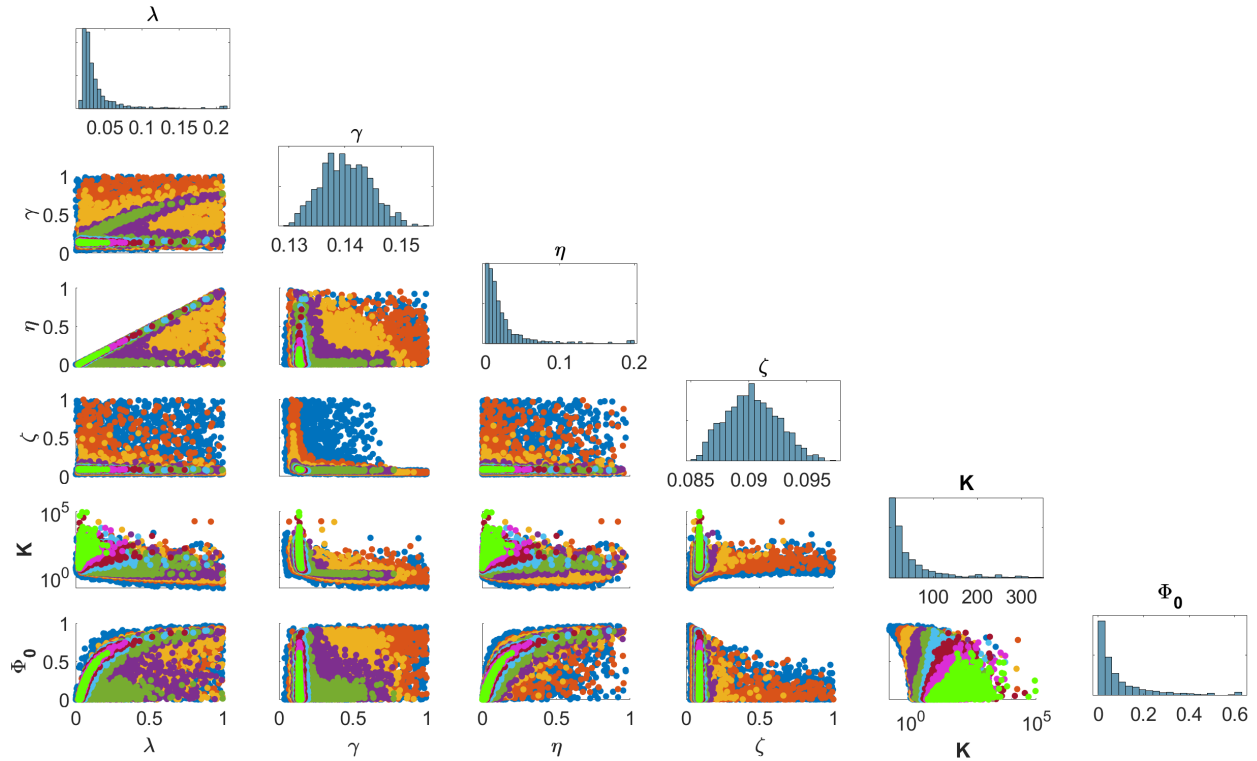


Figure 4. Visualisation of the pairwise posterior distributions resulting from the ABC SMC algorithm corresponding to fitting the two compartment model to the first patient in our clinical dataset, corresponding to the top left panel in Figure 3. The successive populations of particles from each iteration of the ABC SMC algorithm appear as contours in the posterior parameter space with the lime green points marking the most likely regions of parameter space from the posterior distribution. The histograms represent the marginal posterior distributions for each model parameter. $\Phi_0 = N_0/(N_0 + V_0)$ represents the initial necrotic fraction.

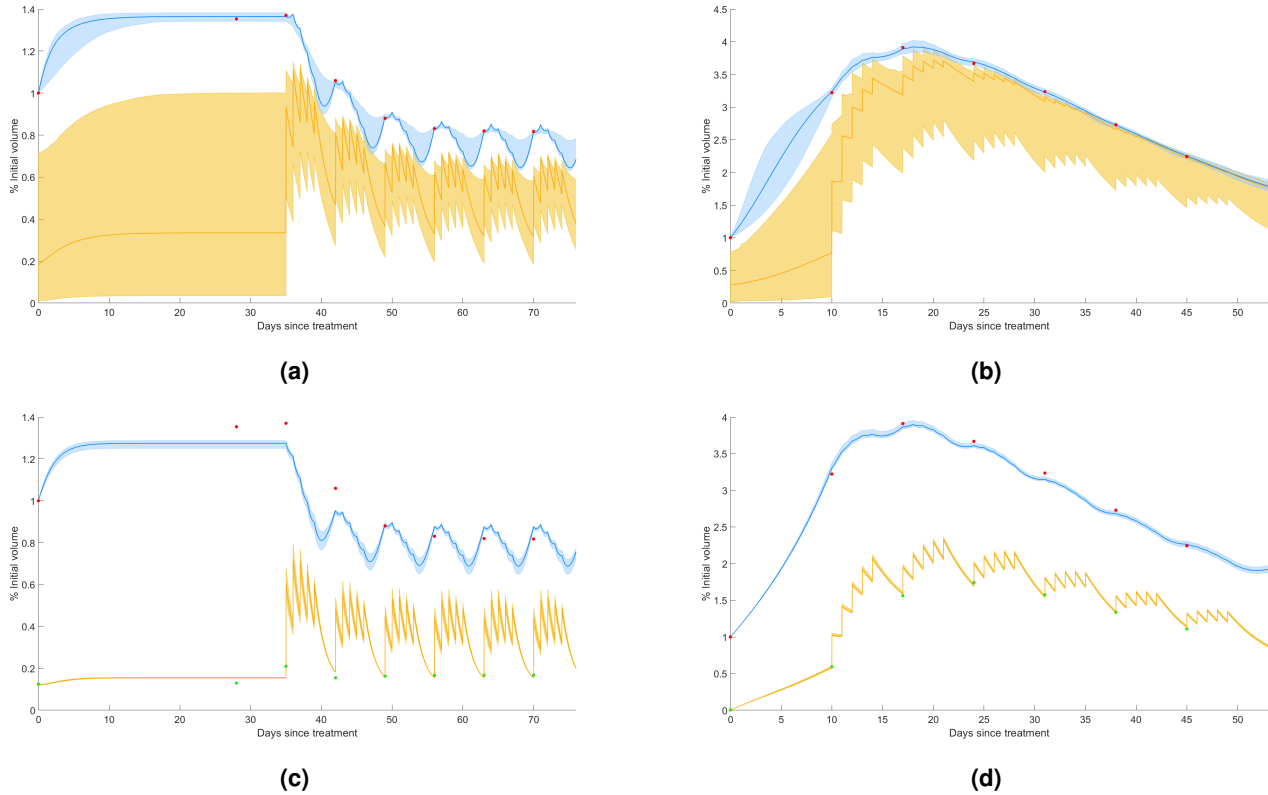


Figure 5. Results from fitting the two compartment model, Equations (2) and (3), to synthetic datasets generated from the multiphase model using the ABC SMC algorithm (see supplementary material for further details). Panels (a) and (c) correspond to data representing the response plateau case, while panels b) and d) use data exhibiting the pseudo-progression case (cf. Figure 1). The total tumour volume and underlying necrotic volume corresponding to simulations using the best-fitting parameter sets are shown by the blue and yellow curves, respectively. 95% credible intervals for the total tumour volume (blue regions) and underlying necrotic volume (yellow regions) at each time point are obtained by sampling 120 parameter combinations from the posterior distributions and simulating Equations (2) and (3). The synthetic data points for total tumour volume are marked by the red dots. In panels c) and d) green dots correspond to additional data points for the necrotic volume which are used for model calibration.

Fitting the two compartment model to just half of this synthetic dataset using simply the total tumour volume, we again reproduce the effects observed in the previous section whereby the lack of identifiability is represented in the width of the 95% credible intervals for the dead material compartment (Figures 5a and 5b). If, however, we use the full set of data generated including the necrotic volume fraction, then we observe that both the total tumour volume and the underlying composition dynamics are now constrained by the calibration data (Figures 5c and 5d). We note that in Figure 5c for the plateau case, the fit to the GTV data is slightly compromised in favour of a better overall fit. This is not surprising since the multiphase model provides a far more complex, mechanistic description of the effects of heterogeneity of the tumour micro-environment such that it would be unreasonable to expect the simplicity of the two compartment model to completely emulate this. In turn, of course, the multiphase model is a simplification of the biology *in vivo*. In reality, such a discrepancy is likely to be within reasonable noise bounds encompassed within the data and biological variability. This fit also represents an improvement upon the fits obtained using phenomenological scalar ODEs for such characteristic responses (cf. Figure 2).

However, the rationale for using mathematical models extends beyond simply describing observed clinical data. Indeed, for a mathematical model to be of use it should be descriptive and identifiable with respect to calibration data such that predictions can be made sufficiently early during the course of a patient's treatment. As such, we are led to extend these experimental design questions to understand how much data are needed to sufficiently constrain model predictions. To address this, we temporally split our synthetic datasets, using the initial time points for model calibration with the remaining data points serving for model validation purposes.

In Figure 6, we present an example using synthetic data from a multiphase simulation exhibiting a fast response to treatment.

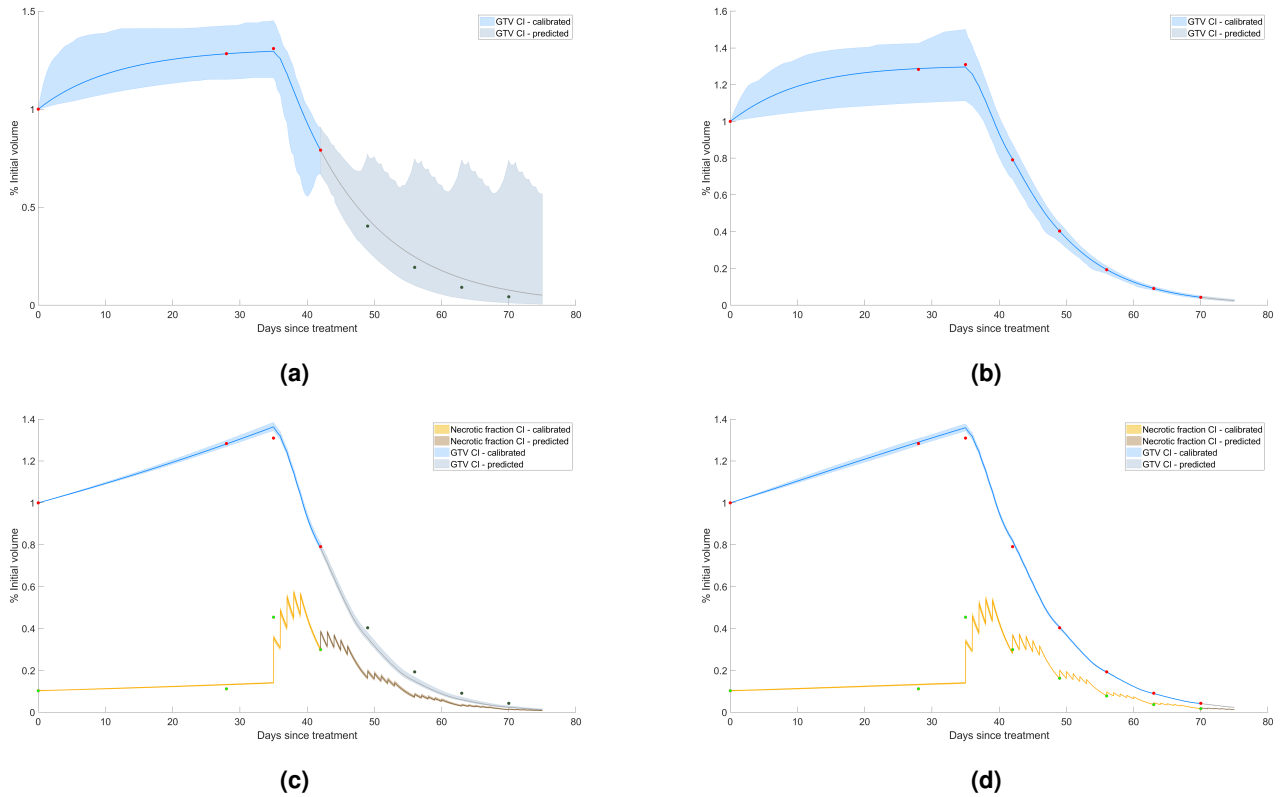


Figure 6. Results from fitting the two compartment model given by Equations (2) and (3) to synthetic data which qualitatively exhibits a fast response to radiotherapy (see supplementary material for further details of the generation of synthetic data). The synthetic data points are split such that red points correspond to tumour volume measurements used for model calibration whilst dark green points are used for validation. In panels (a) and (c) the calibration dataset includes all time points pre-treatment and a time point after the first week of the radiotherapy protocol, whereas all time points are included for panels (b) and (d). In panels (c) and (d), light green data points representing the underlying necrotic volume within the tumour are additionally used as part of the calibration dataset. The total tumour volume and underlying necrotic volume corresponding to simulations using the best-fitting parameter sets are shown by the blue and yellow curves, respectively. 95% credible intervals for the total tumour volume (blue regions) and underlying necrotic volume (yellow regions) at each time point are obtained by sampling 120 parameter combinations from the posterior distributions and simulating Equations (2) and (3). Grey regions represent the 95% credible intervals for the posterior predictive distribution which extend to time points beyond the data used for model calibration.

In the split dataset we use the pre-treatment measurements and a single time point after the first week of treatment to calibrate the two compartment model (panels 6a and 6c). The results are compared to those from fitting the model to the complete dataset (panels 6b and 6d). We repeat this exercise for both the scenario in which we simply have GTV measurements and our hypothetical scenario which is supplemented with tumour composition measurements. In Figure 6a, we observe that the calibration data points are not sufficient to accurately constrain the posterior predictions for the tumour volume at the end of the simulated radiotherapy protocol. Furthermore, the lack of parameter identifiability is demonstrated by the appearance of two qualitatively different predicted responses - namely, the fast response and plateau cases. These qualitatively different predictions would also result in significant quantitative differences between the predictions of GTV at the end of the radiotherapy protocol. In contrast, in Figure 6c, we observe that by using tumour composition data we are able to constrain the model predictions to the true qualitative dynamics using the same temporal resolution. In this case, the model is now able to accurately predict the tumour volume at the end of treatment from data points after just the first week of treatment.

Such discussion of the results in Figures 6a and 6c is perhaps not a fair comparison. In particular, the calibration dataset used in Figure 6a contains half the number of points of that in Figure 6c and, furthermore, is smaller in size than the total number of model parameters to be estimated. It is thus not surprising that the model is not identifiable in this setup. Therefore a comparison of Figures 6b and 6c is perhaps more reasonable. In this case we notice that, for the same number of data points

used for calibration, we obtain similar fits to the synthetic data and similar model predicted outcomes. Of course, in the case of Figure 6b, the prediction merely extends to the final week of the simulated protocol after the final data point. While both setups yield similar model predictions, the scenario in Figure 6c does so at a time point at which such predictions may hypothetically be advantageous in the determination of adaptive treatment protocols. Indeed, a further benefit afforded by the increased identifiability in this scenario would be realised as a reduced uncertainty in subsequent predictions of alternative protocols.

Discussion

The development of predictive mathematical models for determining patient-specific radiotherapy response in the clinic faces two contrasting challenges - incorporate sufficient detail to accurately describe the underlying biological complexity whilst maintaining parameter identifiability with respect to the clinical data typically available for model calibration. Such data are often limited, which commonly limits models to simple, phenomenological descriptions of the tumour dynamics. Advances in radiomics may provide quantitative imaging that identifies different tumor microenvironments, or habitats, that help calibrate and validate more complex models in the future^{54,55}. Motivated by previous work, in this paper we have presented results which suggest that incorporating some notion of heterogeneity in the tumour micro-environment into existing phenomenological ODE models may improve the range of dynamics captured by such models. Indeed, the example two compartment model presented here may reproduce the different qualitative gross tumour volume (GTV) dynamics throughout treatment observed in our patient cohort and characterised in Figure 1. This represents an improvement upon previously proposed scalar ODEs which may be unable to capture subsets of the entire patient population which exhibit more complex behaviours.

However, these results only address one of the two aforementioned concerns which are essential to the development of predictive mathematical models. Inherent in the extension of simple, phenomenological models in this way to include more biological detail is the introduction of additional model parameters. Such an increase in the dimensionality of the model parameter space places stronger requirements on the data necessary for model calibration to ensure identifiability. Furthermore, we note that simply increasing the temporal resolution of the data may not be sufficient to ensure identifiability. Given the limitations of the data commonly available for model calibration, parameter values for models of this complexity are likely to be *practically unidentifiable*. Despite the good fit to measurements of overall tumour volume, analysis of simulated trajectories obtained from sampling parameter sets from the posterior distribution showed a large variation in estimates of the underlying tumour composition dynamics. In light of this, model predictions from compartmental models calibrated in the absence of spatial data should be treated with caution. Results of our previous modelling work suggest that heterogeneity in tumour composition may affect the qualitative response to radiotherapy²¹. Consequently, we anticipate that uncertainty due to inadequate calibration data may lead to spurious predictions in these cases. This may be particularly pertinent when simulating and comparing the predictions for alternative or adaptive treatment protocols.

The accuracy of all model predictions is highly influenced by two sources of error, that of the model itself, and the noise inherent within the data points. In this paper we have largely focused attention on the error of the model, which should be minimised by incorporating as much biological detail as possible while giving careful consideration to the identifiability issues discussed. However, it should be noted that error in the data points used for model calibration may also have a significant effect on the accuracy of model predictions. Such effects are likely to be exacerbated in the case of limited data as is typically the case here. An understanding of the influence of these sources of error further the need for appropriate identifiability analysis and understanding of the model parameter space. Moreover caution should be taken when interpreting results in the absence of such analysis or where a single, 'optimal' set of parameters is determined, since this may lead to spurious predictions of radiosensitivity¹⁷ and unrealistic parameter regimes⁵⁶.

In silico data from a more complex model of tumour growth and radiotherapy response were used to serve as a ground truth to approach these questions of experimental design. The synthetic data allowed us to consider alternative spatial metrics of tumour composition in addition to the GTV measurements currently used. In our two compartment model example, while increasing temporal resolution of GTV would not have improved identifiability, additional measurements of necrotic tumour volume would allow for appropriate constraint of model parameters. Thus, more sophisticated imaging techniques may allow for appropriate calibration of more complex mathematical models, without the need for additional time points. Furthermore, such data may allow for more accurate predictions of post-treatment GTV at earlier times, and hence predictions for adaptive protocols may be considered in a timely manner. While the data collection paradigm considered here is hypothetical, advances in imaging technologies are making more complex measurements of the tumour micro-environment *in vivo* feasible⁵⁷⁻⁵⁹, although this is not routinely done since the use of mathematical models is currently not of consideration in the clinic.

However, it is also clear that for certain subsets of patients, such as those we classified as either 'fast' or 'poor' responders to treatment (cf. Figure 1), the simpler, scalar ODE models such as the PSI model¹² used for comparison here may provide adequate model predictions and characterization of patient response. As such, for these patients, the use of more sophisticated imaging techniques may not be necessary. Thus a direction for future work in the use of models such as the PSI model may focus on the stratification of the patient population and how to identify those for whom simpler models may be sufficient at an

early stage.

The results presented in this paper highlight the simultaneous need for the use of detailed models and more sophisticated data metrics to accurately predict the range of responses to radiotherapy observed across the entire patient population. Further work in this area may benefit from a more rigorous analysis of the approach to experimental design and the examples shown here with regards to model calibration. Such analyses should also consider more precisely how model predictions for alternative protocols are affected in order to further advance the translatability of such models for use in the clinic.

The analysis in this paper may also be extended to address the influence on parameter inference of noise levels in the synthetically-generated necrotic data. The use of a more comprehensive clinical dataset in the future will allow for a more detailed treatment of the error model and a more robust characterisation and estimation of the noise in the data. While such extensions are beyond the scope of this paper and left as future work, they will not change the key finding that tumour volume data alone are not sufficient to properly calibrate the two compartment model and that spatial data are necessary to improve this.

There are numerous approaches and techniques which may be employed for performing parameter estimation^{47–50}. In this paper we do not advocate for one specific method or algorithm over another, but rather for careful consideration of both identifiability and uncertainty quantification in this context for understanding the requirements for an appropriate calibration dataset and to avoid erroneous conclusions and predictions arising from an improperly calibrated model. Such analysis may be achieved by using a number of different algorithms designed for this purpose. Confidence intervals for both parameter estimates and predictions may be derived in either a frequentist or a Bayesian framework and, as such, the choice of approach is not of critical importance here.

In this paper we have utilised a Bayesian approach to parameter estimation through which analysis of the posterior parameter distributions in both a marginal and pairwise manner (Figure 4) indicated identifiability issues in our model. A key area for future work will include the use of a more comprehensive clinical dataset with an increased number of patients and which includes spatial data points. Such a dataset would allow for the use of a more informative population prior to more fully leverage the Bayesian framework which may then be updated on an individual and adaptive basis for making personalized predictions. Population approaches such as these have been proposed and successfully applied for similar applications to incorporate inter-individual variability^{60–62}.

The use of clinical imaging to measure tumour and normal tissue physiology (e.g. cell density, proliferation, hypoxia) is a rapidly advancing field^{57–59}. These new techniques, combined with advanced radiomics approaches, may soon provide temporal data of tumour composition with which to parametrise such models. The validation of the approach presented in this paper, when applied to analyse such data, is an important avenue for future work.

References

1. Fowler, J. F. Development of radiobiology for oncology—a personal view. *Phys. Medicine Biol.* **51**, R263–R286, DOI: [10.1088/0031-9155/51/13/R16](https://doi.org/10.1088/0031-9155/51/13/R16) (2006).
2. Caudell, J. J. *et al.* The future of personalised radiotherapy for head and neck cancer. *The Lancet Oncol.* **18**, e266–e273, DOI: [10.1016/S1470-2045\(17\)30252-8](https://doi.org/10.1016/S1470-2045(17)30252-8) (2017).
3. Scott, J. G. *et al.* A Genome-Based Model for Adjusting Radiotherapy Dose (GARD): A Retrospective, Cohort-Based Study. *Lancet Oncol.* **18**, 202–211, DOI: [10.1016/S1470-2045\(16\)30648-9](https://doi.org/10.1016/S1470-2045(16)30648-9) (2017).
4. Sunassee, E. D. *et al.* Proliferation Saturation Index in an Adaptive Bayesian Approach to Predict Patient-Specific Radiotherapy Responses. *Int. J. Radiat. Biol.* **95**, 1421–1426, DOI: [10.1080/09553002.2019.1589013](https://doi.org/10.1080/09553002.2019.1589013) (2019).
5. Enderling, H., Lopez Alfonso, J. C., Moros, E., Caudell, J. J. & Harrison, L. B. Integrating Mathematical Modeling Into the Roadmap for Personalized Adaptive Radiation Therapy. *Trends Cancer* **5**, 467–474, DOI: [10.1016/j.trecan.2019.06.006](https://doi.org/10.1016/j.trecan.2019.06.006) (2019).
6. Collis, J. *et al.* Bayesian Calibration, Validation and Uncertainty Quantification for Predictive Modelling of Tumour Growth: A Tutorial. *Bull. Math. Biol.* **79**, 939–974, DOI: [10.1007/s11538-017-0258-5](https://doi.org/10.1007/s11538-017-0258-5) (2017).
7. Yankeelov, T. E. *et al.* Clinically Relevant Modeling of Tumor Growth and Treatment Response. *Sci. Transl. Medicine* **5**, 187ps9–187ps9, DOI: [10.1126/scitranslmed.3005686](https://doi.org/10.1126/scitranslmed.3005686) (2013). NIHMS150003.
8. Brady, R. & Enderling, H. Mathematical Models of Cancer: When to Predict Novel Therapies, and When Not to. *Bull. Math. Biol.* **81**, 3722–3731, DOI: [10.1007/s11538-019-00640-x](https://doi.org/10.1007/s11538-019-00640-x) (2019).
9. Stevens, C., Bondy, S. J. & Loblaw, D. A. Wait times in prostate cancer diagnosis and radiation treatment. *Can. Urol. Assoc. journal = J. de l'Association des urologues du Can.* **4**, 243–8 (2010).
10. Sharma, S. *et al.* Clinical impact of prolonged diagnosis to treatment interval (DTI) among patients with oropharyngeal squamous cell carcinoma. *Oral Oncol* **56**, 17–24, DOI: [10.1016/j.oraloncology.2016.02.010](https://doi.org/10.1016/j.oraloncology.2016.02.010) (2016).

11. Wang, L. *et al.* Time to Treatment in Patients With Stage III Non–Small Cell Lung Cancer. *Int. J. Radiat. Oncol.* **74**, 790–795, DOI: [10.1016/j.ijrobp.2008.08.039](https://doi.org/10.1016/j.ijrobp.2008.08.039) (2009). NIHMS150003.
12. Prokopiou, S. *et al.* A proliferation saturation index to predict radiation response and personalize radiotherapy fractionation. *Radiat. Oncol.* **10**, 159, DOI: [10.1186/s13014-015-0465-x](https://doi.org/10.1186/s13014-015-0465-x) (2015).
13. Rockne, R. C. & Frankel, P. Mathematical Modeling in Radiation Oncology. In Wong, J. Y. C., Schultheiss, T. E. & Radany, E. H. (eds.) *Advances in Radiation Oncology*, chap. 12, 255–271 (Springer International Publishing, 2017).
14. McAneney, H. & O’Rourke, S. F. C. Investigation of various growth mechanisms of solid tumour growth within the linear-quadratic model for radiotherapy. *Phys. medicine biology* **52**, 1039–1054, DOI: [10.1088/0031-9155/52/4/012](https://doi.org/10.1088/0031-9155/52/4/012) (2007).
15. Poleszczuk, J. *et al.* Predicting Patient-Specific Radiotherapy Protocols Based on Mathematical Model Choice for Proliferation Saturation Index. *Bull. Math. Biol.* **80**, 1195–1206, DOI: [10.1007/s11538-017-0279-0](https://doi.org/10.1007/s11538-017-0279-0) (2018).
16. Sachs, R. K., Hlatky, L. R. & Hahnfeldt, P. Simple ODE models of tumor growth and anti-angiogenic or radiation treatment. *Math. Comput. Model.* **33**, 1297–1305, DOI: [10.1016/S0895-7177\(00\)00316-2](https://doi.org/10.1016/S0895-7177(00)00316-2) (2001).
17. Tariq, I., Chen, T., Kirkby, N. F. & Jena, R. Modelling and Bayesian adaptive prediction of individual patients’ tumour volume change during radiotherapy. *Phys. medicine biology* **61**, 2145–2161, DOI: [10.1088/0031-9155/61/5/2145](https://doi.org/10.1088/0031-9155/61/5/2145) (2016).
18. Chvetsov, A. V. Tumor response parameters for head and neck cancer derived from tumor-volume variation during radiation therapy. *Med. Phys.* **40**, 034101, DOI: [10.1118/1.4789632](https://doi.org/10.1118/1.4789632) (2013).
19. Rockne, R. *et al.* Predicting the efficacy of radiotherapy in individual glioblastoma patients in vivo: a mathematical modeling approach. *Phys. medicine biology* **55**, 3271–3285, DOI: [10.1088/0031-9155/55/12/001](https://doi.org/10.1088/0031-9155/55/12/001) (2010).
20. Lewin, T. D., Maini, P. K., Moros, E. G., Enderling, H. & Byrne, H. M. The Evolution of Tumour Composition During Fractionated Radiotherapy: Implications for Outcome. *Bull. Math. Biol.* DOI: [10.1007/s11538-018-0391-9](https://doi.org/10.1007/s11538-018-0391-9) (2018).
21. Lewin, T. D. *et al.* The importance of dead material within a tumour on the dynamics in response to radiotherapy. *Phys. Medicine Biol.* **65**, ab4c27, DOI: [10.1088/1361-6560/ab4c27](https://doi.org/10.1088/1361-6560/ab4c27) (2020).
22. Rockne, R. C. *et al.* A patient-specific computational model of hypoxia-modulated radiation resistance in glioblastoma using (18)F-FMISO-PET. *J. Royal Soc. Interface* **12**, 20141174, DOI: [10.1098/rsif.2014.1174](https://doi.org/10.1098/rsif.2014.1174) (2015).
23. Ribba, B., Colin, T. & Schnell, S. A multiscale mathematical model of cancer, and its use in analyzing irradiation therapies. *Theor. biology & medical modelling* **3**, 7, DOI: [10.1186/1742-4682-3-7](https://doi.org/10.1186/1742-4682-3-7) (2006). 0606035.
24. Chvetsov, A. V., Yartsev, S., Schwartz, J. L. & Mayr, N. Assessment of interpatient heterogeneity in tumor radiosensitivity for nonsmall cell lung cancer using tumor-volume variation data. *Med. Phys.* **41**, 064101, DOI: [10.1118/1.4875686](https://doi.org/10.1118/1.4875686) (2014).
25. Chvetsov, A. V., Dong, L., Palta, J. R. & Amdur, R. J. Tumor-Volume Simulation During Radiotherapy for Head-and-Neck Cancer Using a Four-Level Cell Population Model. *Int. J. Radiat. Oncol. Biol. Phys.* **75**, 595–602, DOI: [10.1016/j.ijrobp.2009.04.007](https://doi.org/10.1016/j.ijrobp.2009.04.007) (2009).
26. Wang, P. & Feng, Y. A mathematical model of tumor volume changes during radiotherapy. *TheScientificWorldJournal* **2013**, 181070, DOI: [10.1155/2013/181070](https://doi.org/10.1155/2013/181070) (2013).
27. Rockne, R., Alvord, E. C., Rockhill, J. K. & Swanson, K. R. A mathematical model for brain tumor response to radiation therapy. *J. Math. Biol.* **58**, 561–578, DOI: [10.1007/s00285-008-0219-6](https://doi.org/10.1007/s00285-008-0219-6) (2009).
28. Enderling, H., Park, D., Hlatky, L. & Hahnfeld, P. The importance of spatial distribution of stemness and proliferation state in determining tumor radioresponse. *Math. Model. Nat. Phenom.* **4**, 117–133, DOI: [10.1051/mmnp/20094305](https://doi.org/10.1051/mmnp/20094305) (2013).
29. Gao, X., McDonald, J. T., Hlatky, L. & Enderling, H. Acute and Fractionated Irradiation Differentially Modulate Glioma Stem Cell Division Kinetics. *Cancer Res.* **73**, 1481–1490, DOI: [10.1158/0008-5472.CAN-12-3429](https://doi.org/10.1158/0008-5472.CAN-12-3429) (2013).
30. Alfonso, J. C. L., Jagiella, N., Nunez, L., Herrero, M. A. & Drasdo, D. Estimating dose painting effects in radiotherapy: a mathematical model. *PLoS one* **9**, e89380, DOI: [10.1371/journal.pone.0089380](https://doi.org/10.1371/journal.pone.0089380) (2014).
31. Powathil, G. G., Munro, A. J., Chaplain, M. A. & Swat, M. Bystander effects and their implications for clinical radiation therapy: Insights from multiscale in silico experiments. *J. Theor. Biol.* **401**, 1–14, DOI: [10.1016/j.jtbi.2016.04.010](https://doi.org/10.1016/j.jtbi.2016.04.010) (2016). 1407.0867.
32. Powathil, G. G., Adamson, D. J. & Chaplain, M. A. Towards Predicting the Response of a Solid Tumour to Chemotherapy and Radiotherapy Treatments: Clinical Insights from a Computational Model. *PLoS Comput. Biol.* **9**, DOI: [10.1371/journal.pcbi.1003120](https://doi.org/10.1371/journal.pcbi.1003120) (2013).

33. Richard, M., Kirkby, K. J., Webb, R. P. & Kirkby, N. F. A mathematical model of response of cells to radiation. *Nucl. Instruments Methods Phys. Res. Sect. B: Beam Interactions with Mater. Atoms* **255**, 18–22, DOI: [10.1016/j.nimb.2006.11.077](https://doi.org/10.1016/j.nimb.2006.11.077) (2007).
34. Zaider, M. & Minerbo, G. N. Tumour control probability : a formulation applicable to any temporal protocol of dose delivery. *Phys. medicine biology* **45**, 279–293 (2000).
35. Zaider, M. & Hanin, L. Tumor control probability in radiation treatment. *Med. Phys.* **38**, 574–583, DOI: [10.1118/1.3521406](https://doi.org/10.1118/1.3521406) (2011).
36. Bobadilla, A. V. P., Maini, P. K. & Byrne, H. A stochastic model for tumour control probability that accounts for repair from sublethal damage. *Math. Medicine Biol.* **35**, 181–202, DOI: [10.1093/imammb/dqw024](https://doi.org/10.1093/imammb/dqw024) (2018).
37. O'Rourke, S. F. C., McAneney, H. & Hillen, T. Linear quadratic and tumour control probability modelling in external beam radiotherapy. *J. Math. Biol.* **58**, 799–817, DOI: [10.1007/s00285-008-0222-y](https://doi.org/10.1007/s00285-008-0222-y) (2009).
38. Gong, J., Dos Santos, M. M., Finlay, C. & Hillen, T. Are more complicated tumour control probability models better? *Math. Medicine Biol.* **30**, 1–19, DOI: [10.1093/imammb/dqr023](https://doi.org/10.1093/imammb/dqr023) (2013).
39. Hanin, L. G. A stochastic model of tumor response to fractionated radiation: Limit theorems and rate of convergence. *Math. Biosci.* **191**, 1–17, DOI: [10.1016/j.mbs.2004.04.003](https://doi.org/10.1016/j.mbs.2004.04.003) (2004).
40. Gerlee, P. The model muddle: In search of tumor growth laws. *Cancer Res.* **73**, 2407–2411, DOI: [10.1158/0008-5472.CAN-12-4355](https://doi.org/10.1158/0008-5472.CAN-12-4355) (2013). [1209.3170](https://doi.org/10.1209.3170).
41. Murphy, H., Jaafari, H. & Dobrovolsky, H. M. Differences in predictions of ODE models of tumor growth: a cautionary example. *BMC Cancer* **16**, 163, DOI: [10.1186/s12885-016-2164-x](https://doi.org/10.1186/s12885-016-2164-x) (2016).
42. Benzekry, S. *et al.* The importance of spatial distribution of stemness and proliferation state in determining tumor radioresponse. *PLoS Comput. Biol.* **10**, e1003800, DOI: [10.1371/journal.pcbi.1003800](https://doi.org/10.1371/journal.pcbi.1003800) (2014).
43. Norton, L., Simon, R., Brereton, H. D. & Bogden, A. E. Predicting the course of gompertzian growth. *Nature* **264**, 542–545 (1976).
44. Benzekry, S. *et al.* Classical mathematical models for description and prediction of experimental tumor growth. *PLoS Comput. Biol.* **10**, e1003800 (2014).
45. Zahid, M. U. *et al.* Proliferation saturation index to characterize response to rt and evaluate altered fractionation in head and neck cancer. *Appl. Radiat. Oncol.* **10**, 18–25 (2021).
46. Lewin, T. D., Maini, P. K., Moros, E. G., Enderling, H. & Byrne, H. M. A three phase model to investigate the effects of dead material on the growth of avascular tumours. *Math. Model. Nat. Phenom.* **15**, 22, DOI: [10.1051/mmnp/2019039](https://doi.org/10.1051/mmnp/2019039) (2020).
47. Andradottir, S. A review of simulation optimization techniques. *1998 Winter Simul. Conf. Proc. (Cat. No.98CH36274)* **1**, 151–158, DOI: [10.1109/WSC.1998.744910](https://doi.org/10.1109/WSC.1998.744910) (1998).
48. Park, L. J., Park, C. H., Park, C. & Lee, T. Application of genetic algorithms to parameter estimation of bioprocesses. *Med. & Biol. Eng. & Comput.* **35**, 47–49, DOI: [10.1007/BF02510391](https://doi.org/10.1007/BF02510391) (1997).
49. Gelman, A., Carlin, J. B., Stern, H. S. & Rubin, D. B. *Bayesian Data Analysis* (2014).
50. Lavielle, M. *Mixed effects models for the population approach: models, tasks, methods and tools* (CRC press, 2014).
51. Toni, T., Welch, D., Strelkowa, N., Ipsen, A. & Stumpf, M. P. H. Approximate Bayesian computation scheme for parameter inference and model selection in dynamical systems. *J. Royal Soc. Interface / Royal Soc.* **6**, 187–202, DOI: [10.1098/rsif.2008.0172](https://doi.org/10.1098/rsif.2008.0172) (2009). [0901.1925](https://doi.org/10.1098/rsif.2008.0172).
52. Toni, T. & Stumpf, M. P. H. Simulation-based model selection for dynamical systems in systems and population biology. *Bioinformatics* **26**, 104–110, DOI: [10.1093/bioinformatics/btp619](https://doi.org/10.1093/bioinformatics/btp619) (2009).
53. Alahmadi, A. A., Flegg, J. A., Cochrane, D. G., Drovandi, C. C. & Keith, J. M. A comparison of approximate versus exact techniques for bayesian parameter inference in nonlinear ordinary differential equation models. *Royal Soc. open science* **7**, 191315 (2020).
54. Gatenby, R. A., Grove, O. & Gillies, R. J. Quantitative imaging in cancer evolution and ecology. *Radiology* **269**, 8–15, DOI: [10.1148/radiol.13122697](https://doi.org/10.1148/radiol.13122697) (2013).
55. Gillies, R. J. & Balagurunathan, Y. Perfusion MR Imaging of Breast Cancer: Insights Using "Habitat Imaging". *Radiology* **288**, 36–37, DOI: [10.1148/radiol.2018180271](https://doi.org/10.1148/radiol.2018180271) (2018).

56. Leder, K. *et al.* Mathematical modeling of pdgf-driven glioblastoma reveals optimized radiation dosing schedules. *Cell* **156**, 603–616, DOI: [10.1016/j.cell.2013.12.029](https://doi.org/10.1016/j.cell.2013.12.029) (2014). [NIHMS150003](#).
57. Sun, Y. *et al.* Voxel-wise prostate cell density prediction using multiparametric magnetic resonance imaging and machine learning. *Acta Oncol.* **57**, 1540–1546, DOI: [10.1080/0284186X.2018.1468084](https://doi.org/10.1080/0284186X.2018.1468084) (2018).
58. Salem, A. *et al.* Oxygen-enhanced MRI Is Feasible, Repeatable, and Detects Radiotherapy-induced Change in Hypoxia in Xenograft Models and in Patients with Non-small Cell Lung Cancer. *Clin. Cancer Res.* **25**, 3818–3830, DOI: [10.1158/1078-0432.ccr-18-3932](https://doi.org/10.1158/1078-0432.ccr-18-3932) (2019).
59. Rockne, R. C. *et al.* The 2019 mathematical oncology roadmap. *Phys. Biol.* **16**, 041005, DOI: [10.1088/1478-3975/ab1a09](https://doi.org/10.1088/1478-3975/ab1a09) (2019).
60. Bruno, R. *et al.* Progress and opportunities to advance clinical cancer therapeutics using tumor dynamic models. *Clin. Cancer Res.* **26**, 1787–1795 (2020).
61. Claret, L. *et al.* Model-based prediction of phase iii overall survival in colorectal cancer on the basis of phase ii tumor dynamics. *J. Clin. Oncol.* **27**, 4103–4108 (2009).
62. Ribba, B. *et al.* A tumor growth inhibition model for low-grade glioma treated with chemotherapy or radiotherapy. *Clin. Cancer Res.* **18**, 5071–5080 (2012).

Acknowledgements

This work was funded in part by the Engineering and Physical Sciences Research Council (grant number EP/G037280/1). TL would also like to thank the Moffitt Cancer Center, where some of this work was undertaken, for their hospitality.

Author contributions statement

TL wrote the main manuscript text and prepared the figures. JC collected and provided the clinical data. PM, EM, HE and HM supervised the project. All authors were involved in the methodological development and investigation and reviewed the manuscript.

Additional information

The authors declare no competing interests.

Using mathematical modelling to identify data requirements for increased prediction accuracy in radiotherapy: Supplementary material

Thomas D. Lewin^{1,*}, Philip K. Maini¹, Eduardo G. Moros², Jimmy Caudell², Heiko Enderling^{2,3,*}, and Helen M. Byrne^{1,*}

¹Wolfson Centre for Mathematical Biology, Mathematical Institute, University of Oxford, UK

²Department of Radiation Oncology, H. Lee Moffitt Cancer Center & Research Institute, USA

³Department of Integrated Mathematical Oncology, H. Lee Moffitt Cancer Center & Research Institute, USA
*tomlewin@hotmail.co.uk or heiko.enderling@moffitt.org or helen.byrne@maths.ox.ac.uk

Parameter sweep of two compartment model dynamics

In this section we present the results of a parameter sweep of the two compartment model and visualise the range of dynamics captured by the model. For convenience we restate the model equations below:

$$\frac{dV}{dt} = \lambda V \left(1 - \frac{V}{K}\right) - \eta V - \gamma \sum_{i=1}^n V \delta(t - t_i), \quad (1)$$

$$\frac{dN}{dt} = \eta V - \zeta N + \gamma \sum_{i=1}^n V \delta(t - t_i). \quad (2)$$

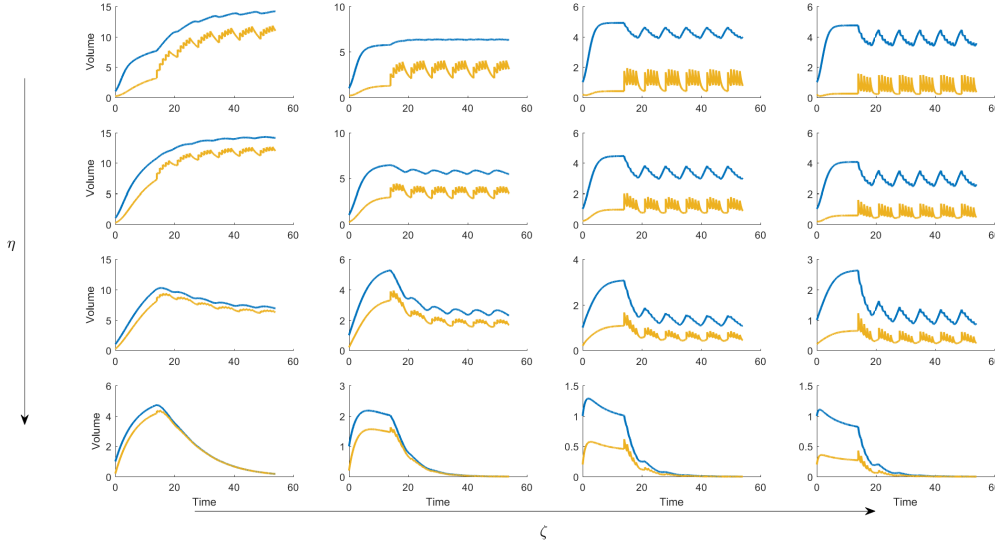
When coupled with appropriate initial conditions for $V(0)$ and $N(0)$, Equations (1) and (2) define the two compartment model proposed in this paper, with the total tumour volume at time t given by $Y(t) := V(t) + N(t)$.

It is straightforward to show that, in the absence of radiotherapy, the growth kinetics result in a steady state total tumour volume, $Y = \tilde{K}$, given by

$$\tilde{K} = K \left(1 - \frac{\eta}{\lambda}\right) \left(1 + \frac{\eta}{\zeta}\right). \quad (3)$$

The necrotic fraction, defined to be $\frac{N}{Y}$, at equilibrium is given by $\frac{\eta}{\eta + \zeta}$.

We perform a parameter sweep varying the necrosis rate, η , and the decay rate of necrotic material, ζ , in order to determine the qualitative responses exhibited by the model to radiotherapy. In all cases we simulate the standard fractionation protocol for 6 weeks, starting at $t = 14$. In Supplementary Figure S1 we display the results of the parameter sweep. We show how the dynamics of the necrotic volume, N , and total tumour volume, Y , change as η and ζ vary. As expected, increasing the necrosis rate, η , results in smaller tumour volumes post-radiotherapy since the tumour's composition at steady state (in the absence of radiotherapy) contains a larger necrotic fraction and smaller proliferative tumour population. As the rate of necrotic decay, ζ , increases, the trajectories for the overall tumour volume resemble those associated with models which simulate instantaneous cell death upon irradiation, such as the PSI model (c.f. Figure 2 in the main text). Conversely, smaller values of ζ result in less pronounced changes in total tumour volume following irradiation and allow necrotic material to accumulate within the tumour. We note the wider array of qualitative response observed compared to the PSI model and, in particular, note that different parameter regimes may give rise to dynamics which resemble the responses presented in Figure 1 (main text). In particular, varying the value of ζ may give rise to both pseudo-progression behaviour and response plateau dynamics.



Supplementary Figure S1: Results of a parameter sweep for the two compartment model, simulating Equations (1) and (2). Parameters increase in the direction of the arrows with necrosis rate, $\eta \in [0.1, 0.99]$, varying by row, and the decay rate of necrotic material, $\zeta \in [0.1, 2]$, by column. Trajectories for the total tumour volume, Y , and the underlying volume of necrotic material, N , are shown in blue and yellow, respectively. For each simulation the remaining parameter values are held fixed: $\lambda = 1$, $\gamma = 0.3$, $K = 5$, $Y(0) = 1$ and $\Phi(0) = 0.2$. Radiotherapy is simulated for the standard fractionation protocol starting after a 2 week pre-treatment growth period.

Multiphase model for synthetic data generation

In this paper we use synthetic data studies to facilitate investigation of the performance of the two compartment model given by Equations (1) and (2) and to better understand the influence of intratumoural heterogeneity. We use a previously developed multiphase model of tumour growth and radiotherapy response to generate synthetic data from the different qualitative examples used in this paper. Here we briefly describe our multiphase model and state the full system of equations below; the detailed derivation of the model equations is presented in [7, 8].

We consider a three phase model, focussing on the influence of the dead material within the tumour on the overall tumour growth dynamics. The model treats the tumour micro-environment as a continuum, multiphase mixture, comprising three constituent phases: (i) tumour cells, (ii) dying cells and cellular debris, and (iii) extracellular fluid. The second phase is assumed to comprise all non-viable cellular material and cellular debris within the tumour, irrespective of cell death mechanism or stage of decay. As such, this phase represents an ‘averaged’ description of this component of the tumour environment across all of these modes of cell death and is a transitional phase between the viable tumour population and the extracellular fluid. We hereafter refer to this phase as ‘dead material’.

The spatial distribution of each phase is characterised by the volume fractions $\phi_i(\mathbf{x}, t)$ ($i = 1, 2, 3$) for the tumour cell, dead material and extracellular fluid phases, respectively, at spatial point \mathbf{x} and time t . The phase velocities $\mathbf{v}_i(\mathbf{x}, t)$ describe the movement of each phase, and are associated with the phase pressures, $p_i(\mathbf{x}, t)$, and stress tensors, $\boldsymbol{\sigma}_i(\mathbf{x}, t)$. We model the mixture constituents as fluids, with the tumour and dead material phases treated as viscous, while the extracellular fluid is taken to be inviscid. Mass and momentum balances are applied to each phase to determine how the dependent variables evolve over time. Tumour growth is assumed to be oxygen-dependent and so the system of equations is coupled to a reaction-diffusion equation for the oxygen concentration, $c(\mathbf{x}, t)$.

Radiotherapy effects are modelled as an instantaneous mass transfer between the tumour cell and dead material phases at the time of delivery, t_j . Here, $\nu(c)$ encompasses the dependence of radiation-induced cell death on the local oxygen concentration, c , and is related to the dose-dependent cell survival fraction, $SF(d)$, by $\nu = 1 - SF(d)$. Here we assume radiation is delivered with a uniform spatial dose distribution.

The linear-quadratic (LQ) model is commonly used to describe the dose-dependent survival fraction,

$SF(d)$, of tumour cells after irradiation [6]. Various local oxygen concentrations within a tumour yield spatially heterogeneous radiosensitivities. Hypoxic tumour regions respond poorly to irradiation compared with well-oxygenated conditions. The oxygen enhancement ratio (OER; $OER \approx 3$) is established as the conventional extension to the LQ model to account for hypoxia [2, 3, 5]. This yields a step function for radiation sensitivity at the hypoxia threshold, c_H , given by

$$SF(d, c) = \begin{cases} \exp(-\alpha d - \beta d^2) & c \geq c_H \\ \exp\left(-\frac{\alpha}{OER}d - \frac{\beta}{OER^2}d^2\right) & c < c_H. \end{cases} \quad (4)$$

For simplicity, we simulate the model in a symmetrical 1D Cartesian geometry, where $x = 0$ and $x = R(t)$ denote the centre of the tumour and the (dynamic) position of the tumour boundary, respectively. As previously described, the resulting system of equations may be reduced to eliminate the fluid phase volume fraction, ϕ_3 , velocity, v_3 , and global pressure, p , and then be closed by specifying initial and boundary conditions [8]. This yields the multiphase model for radiotherapy response:

Mass conservation

$$\frac{\partial \phi_1}{\partial t} + \frac{\partial}{\partial x}(\phi_1 v_1) = \eta \phi_1 (1 - \phi_1 - \phi_2) H_\epsilon(c - c_H) - \chi \phi_1 H_\epsilon(c_N - c) - \kappa \phi_1 - \sum_j \nu(c) \phi_1 \delta(t - t_j) \quad (5)$$

$$\frac{\partial \phi_2}{\partial t} + \frac{\partial}{\partial x}(\phi_2 v_2) = \chi \phi_1 H_\epsilon(c_N - c) + \kappa \phi_1 - \lambda \phi_2 + \sum_j \nu(c) \phi_1 \delta(t - t_j) \quad (6)$$

Oxygen profile

$$0 = D \frac{\partial^2 c}{\partial x^2} - \Gamma \phi_1 H_\epsilon(c - c_H) \quad (7)$$

Momentum balances

$$0 = \frac{4}{3} \mu_1 (1 - \phi_1) \frac{\partial}{\partial x} \left(\phi_1 \frac{\partial v_1}{\partial x} \right) - \frac{4}{3} \theta_\mu \mu_1 \phi_1 \frac{\partial}{\partial x} \left(\phi_2 \frac{\partial v_2}{\partial x} \right) + d_{12} \phi_1 \phi_2 (v_2 - v_1) \\ - d_{13} \phi_1 (\phi_2 v_2 + (1 - \phi_2) v_1) - \phi_1 (1 - \phi_1) \frac{\partial \Sigma_\phi}{\partial x} + \theta_p \phi_1 \phi_2 \frac{\partial \Sigma_\phi}{\partial x} \quad (8)$$

$$0 = -\frac{4}{3} \mu_1 \phi_2 \frac{\partial}{\partial x} \left(\phi_1 \frac{\partial v_1}{\partial x} \right) + \frac{4}{3} \theta_\mu \mu_1 (1 - \phi_2) \frac{\partial}{\partial x} \left(\phi_2 \frac{\partial v_2}{\partial x} \right) + d_{12} \phi_1 \phi_2 (v_1 - v_2) \\ - d_{23} \phi_2 (\phi_1 v_1 + (1 - \phi_1) v_2) - \theta_p \phi_2 (1 - \phi_2) \frac{\partial \Sigma_\phi}{\partial x} + \phi_1 \phi_2 \frac{\partial \Sigma_\phi}{\partial x} \quad (9)$$

$$\Sigma_\phi(\phi) = \frac{\zeta(\phi - \phi_{min})^2(\phi - \phi^*)}{(1 - \phi)} H(\phi - \phi_{min}) \quad (10)$$

Initial and boundary conditions

$$\frac{dR}{dt} = v_1|_{x=R(t)} \quad (11)$$

$$\frac{\partial c}{\partial x} = 0, \quad v_1 = v_2 = 0 \quad \text{at} \quad x = 0 \quad (12)$$

$$\phi_2^+ = 0, \quad c = c_\infty \quad \text{at} \quad x = R(t) \quad (13)$$

$$\frac{4}{3} \mu_1 \frac{\partial v_1}{\partial x} - \Sigma_\phi(\phi_1 + \theta_\Sigma \phi_2) = \frac{4}{3} \theta_\mu \mu_1 \frac{\partial v_2}{\partial x} - \theta_p \Sigma_\phi(\phi_1 + \theta_\Sigma \phi_2) = 0 \quad \text{at} \quad x = R(t) \quad (14)$$

$$\phi_1 = \tilde{\phi}_1(x), \quad \phi_2 = \tilde{\phi}_2(x), \quad R = R_0 \quad \text{at} \quad t = 0 \quad (15)$$

For a given simulation of Equations (5)-(15), the size of the tumour at time t is thus given by $R(t)$. As such, synthetic data for total tumour volume analogous to the clinical datasets shown in Figure 1 (main text) may be generated with an appropriate selection of time points.

This synthetic dataset may be extended to include measurements of the necrotic volume within the tumour at each time point. We quantify the necrotic fraction from the multiphase simulation by evaluating

$$\bar{\phi}_2(t) = \frac{1}{R(t)} \int_0^{R(t)} \phi_2(x, t) dx, \quad (16)$$

with the necrotic volume thus given by $\bar{\phi}_2(t)R(t)$.

The parameter regimes used for generating the synthetic data in this paper may be found in Table 3 of Lewin *et al.* [7] along with further discussion of the multiphase model dynamics for each case. The synthetic data in Figures 5a and 5c (main text) exhibiting the ‘plateau’ dynamics correspond to parameter set D. The dataset which qualitatively exhibits ‘pseudo-progression’ dynamics in Figures 5b and 5d is generated using the parameter regime E. Finally, the synthetic data used for the example in Figure 6 is obtained by simulating the multiphase model with parameter set B.

The ABC SMC algorithm for model calibration

Approximate Bayesian Computation (ABC) algorithms are a class of Monte Carlo methods that are ‘likelihood-free’; they do not require explicit calculation of the likelihood. This can be useful if the likelihood is difficult (or impossible) to calculate or, for example, if there are errors in the data that can not be easily quantified or estimated.

In this paper we use a Bayesian approach to model calibration known as the Approximate Bayesian Computation Sequential Monte Carlo (ABC SMC) algorithm which combines the approaches of ABC with a sequential version of importance sampling. Below we briefly summarise the algorithm and the particular configurations used in this paper. A more detailed presentation of the algorithm can be found in the original work by Toni *et al.* [9, 10].

In the ABC SMC algorithm, a set of parameter values called *particles*, $\{\theta_i\}$, sampled from the prior distribution, $\pi(\theta)$, is propagated through a sequence of intermediate distributions, $\pi(\theta \mid d(y^*, y) < \epsilon_t)$ for $t = 1, \dots, T$, until it represents a sample from the target distribution at the desired tolerance level ϵ_T . Here, y denotes the dataset and y^* a simulated dataset corresponding to model predictions for the current parameter set. The function $d(\cdot, y)$ thus measures the distance between the dataset and the model simulation. The threshold sequence is chosen such that $\epsilon_1 > \dots > \epsilon_T > 0$ and therefore the distribution of the particles gradually evolves towards the posterior. At each stage, importance sampling is used to generate the subsequent sample with the importance sampling proposal distribution, η_t , being the previous distribution, $\pi(\theta \mid d(y^*, y) < \epsilon_{t-1})$, perturbed by the perturbation kernel, K_t . The full algorithm is shown in Algorithm S1.

Algorithm S1: ABC SMC algorithm [10].

S1 Initialise $\epsilon_1, \dots, \epsilon_T$.
 Set the population indicator $t = 0$.
S2.0 Set the particle indicator $i = 1$.
S2.1 **if** $t = 0$ **then**
 | Sample θ^{**} independently from $\pi(\theta)$
 else
 | Sample θ^* from the previous population $\{\theta_{t-1}^{(i)}\}$ with weights w_{t-1} and perturb the particle
 | to obtain $\theta^{**} \sim K_t(\theta|\theta^*)$, where K_t is a perturbation kernel.
 end
 if $\pi(\theta^{**}) = 0$ **then**
 | Return to **S2.1**.
 end
 Simulate a candidate dataset $x^* \sim f(x|\theta^{**})$.
 if $d(x^*, x_0) \geq \epsilon_t$ **then**
 | Return to **S2.1**.
 end
S2.2 Set $\theta_t^{(i)} = \theta^{**}$ and calculate the weight for the particle $\theta_t^{(i)}$,

$$w_t^{(i)} = \begin{cases} 1 & \text{if } t = 0, \\ \frac{\pi(\theta_t^{(i)})}{\sum_{j=1}^N w_{t-1}^{(j)} K_t(\theta_t^{(j)}, \theta_t^{(i)})} & \text{if } t > 0. \end{cases}$$

if $i < N$ **then**
 | Set $i = i + 1$.
 | Go to **S2.1**.
 end
S3 Normalize the weights.
 if $t < T$ **then**
 | Set $t = t + 1$.
 | Go to **S2.0**.
 end

A simple adaptive method that is most commonly used for determining the threshold at each iteration is the quantile method. Before the start of each iteration, the new value of ϵ is chosen based upon the pre-determined quantile of the distances between the empirical dataset and the simulated data from the previous population. That is, for a pre-determined α , the new threshold ϵ_t is chosen such that $\alpha\%$ of the previous population gives rise to simulated data, y^* , that satisfies $d(y^*, y) < \epsilon_t$.

Alahmadi *et al.* [1] identify that improper consideration of the error model within the ABC SMC algorithm and a choice of ϵ_T that is too small may lead to inaccurate inference of the posterior. To mitigate these concerns we choose ϵ_T such that it is equivalent to a 10% proportional error for each data point.

A judicious choice of the perturbation kernel to be used in the ABC SMC algorithm may enhance the performance of the algorithm. A good perturbation kernel will allow sufficient exploration of the parameter space whilst also achieving a high acceptance rate. Filippi *et al.* [4] propose the use of a multivariate normal perturbation kernels local to the particle that is being perturbed. In this case, the covariance matrix Σ is defined uniquely for each particle in the preceding population. The optimal local covariance matrix for the particle θ_i^{t-1} is then given by

$$\Sigma_{\theta_i^{t-1}} = \int p_{\epsilon_t}(\theta^t | y) (\theta^t - \theta_i^{t-1})(\theta^t - \theta_i^{t-1})^T d\theta^t d\theta^{t-1}, \quad (17)$$

which can be approximated by

$$\Sigma_{\theta_i^{t-1}} \approx \sum_{k=1}^{N_0} \tilde{w}_k (\tilde{\theta}_k - \theta_i^{t-1})(\tilde{\theta}_k - \theta_i^{t-1})^T. \quad (18)$$

In this paper we use the ABC SMC algorithm given by Algorithm S1 with the setup options summarised in Supplementary Table S1. We use the residual sum of squares as a metric for the distance between the model and the data, weighting each residual by the magnitude of the data point.

Algorithm option	Setup used
Threshold schedule method, ϵ_t	Adaptive - 10% quantile
Number of particles	4000
Parameter perturbation kernel type	Multivariate normal optimal local covariance matrix
Growth rate prior, λ	$U(0, 1)$
Death rate prior, γ	$U(0, 1)$
Necrosis rate prior, η	$U(0, \lambda)$
Necrotic decay rate prior, ζ	$U(0, 1)$
Initial tumour volume:carrying capacity prior, $\frac{Y(0)}{K}$	$U(0, 1)$
Initial necrotic fraction prior, $\Phi(0)$	$U(\max(0, 1 - K(1 - \frac{\eta}{\lambda})), \frac{\eta}{\eta + \zeta})$

Supplementary Table S1: Options used for setting up the ABC SMC algorithm.

As a result of the ABC SMC algorithm, we obtain a weighted sample of parameter sets which approximate the true posterior distribution. The posterior predictive distribution for new data, y^* , is defined as

$$p(y^* | y) = \int p(y^* | \theta, y)p(\theta | y)d\theta, \quad (19)$$

and can be obtained for any y^* from the posterior distribution for θ . The posterior predictive distribution allows us to assess the uncertainty in our model predictions given a set of data and a particular quantity of interest. By sampling parameter sets from the posterior distribution and simulating the model we may approximate the posterior predictive distribution and thus generate credible intervals as presented in this paper.

References

- [1] A. A. Alahmadi, J. A. Flegg, D. G. Cochrane, C. C. Drovandi, and J. M. Keith. A comparison of approximate versus exact techniques for bayesian parameter inference in nonlinear ordinary differential equation models. *Royal Society open science*, 7(3):191315, 2020.
- [2] T. Alper and P. Howard-Flanders. Role of Oxygen in Modifying the Radiosensitivity of E. Coli B. *Nature*, 178:978–979, 1956.
- [3] D. J. Carlson, R. D. Stewart, and V. A. Semenenko. Effects of oxygen on intrinsic radiation sensitivity: A test of the relationship between aerobic and hypoxic linear-quadratic (LQ) model parameters. *Medical physics*, 33(9):3105–3115, 2006. doi: 10.1118/1.2229427.
- [4] S. Filippi, C. P. Barnes, J. Cornebise, and M. P. H. Stumpf. On optimality of kernels for approximate Bayesian computation using sequential Monte Carlo. *Statistical Applications in Genetics and Molecular Biology*, 12(1):87–107, 2013. doi: 10.1515/sagmb-2012-0069.
- [5] M. R. Horsman, B. G. Wouters, M. C. Joiner, and J. Overgaard. The oxygen effect and fractionated radiotherapy. In M. C. Joiner and A. J. van der Kogel, editors, *Basic Clinical Radiobiology*. CRC Press, 2009.
- [6] M. Joiner and A. van der Kogel. *Basic Clinical Radiobiology Fourth Edition*. CRC Press, mar 2009. ISBN 1444166689. doi: 10.1201/b13224.
- [7] T. D. Lewin, H. M. Byrne, P. K. Maini, J. J. Caudell, E. G. Moros, and H. Enderling. The importance of dead material within a tumour on the dynamics in response to radiotherapy. *Physics in Medicine and Biology*, 65(1):ab4c27, 2020. ISSN 13616560. doi: 10.1088/1361-6560/ab4c27. URL <https://doi.org/10.1088/1361-6560/ab4c27>.
- [8] T. D. Lewin, P. K. Maini, E. G. Moros, H. Enderling, and H. M. Byrne. A three phase model to investigate the effects of dead material on the growth of avascular tumours. *Mathematical Modelling of Natural Phenomena*, 15:22, 2020. ISSN 0973-5348. doi: 10.1051/mmnp/2019039.

- [9] T. Toni and M. P. H. Stumpf. Simulation-based model selection for dynamical systems in systems and population biology. *Bioinformatics*, 26(1):104–110, 2009. doi: 10.1093/bioinformatics/btp619.
- [10] T. Toni, D. Welch, N. Strelkova, A. Ipsen, and M. P. H. Stumpf. Approximate Bayesian computation scheme for parameter inference and model selection in dynamical systems. *Journal of the Royal Society, Interface / the Royal Society*, 6(31):187–202, 2009. doi: 10.1098/rsif.2008.0172.